JFE TECHNICAL REPORT
No. 27 (Mar. 2022)

Evaluation and Analysis Techniques of Magnetic Materials for EV/HEV Motors

NAKADA Takahiro[*1] NAKANISHI Tadashi[*2]

Abstract:

In this article state-of-the-art technologies developed by JFE Techno-Research are described in the field of measurement and analysis of magnetic functional materials such as electrical steels and permanent magnets, which are key materials determining EV and HEV motor efficiency and performance. Distribution of magnetic flux and field strength around the welded in a stator core are analyzed using needle probes and H coils. AC eddy current loss measurement of sintered Nd-Fe-B magnets using a developed AC magnetizing device revealed that eddy current loss of divided magnet was greatly reduced even without any electrical insulation treatment in the contacting sides of the divided magnets. Measured result was relatively consistent with the results of magnetic FEM analysis. In addition, measurement technique in motor vibration is also featured, which are gaining emerging interest in EV and HEV applications. Motor vibration was analyzed by using a motor evaluation system and a three-dimensional vibration acceleration sensor.

1. Introduction

As protection of the global environment becomes an increasingly urgent issue, production of low environmental load EV/HEV (electric vehicles/hybrid electric vehicles) is continuing to rise. Because the motor is the key factor that determines the energy efficiency of an EV or HEV, low iron loss of motor core materials is required in order to achieve higher efficiency, and high magnetic flux density of motor core materials is also essential for realizing compact size and high torque. JFE Steel has developed various types of outstanding electrical steel sheets to meet these performance requirements[1].

On the other hand, the measured loss of motor cores differs greatly in some cases from estimated result by the electromagnetic field analysis. These differences arise because the magnetic property used in electromagnetic field analyses are measured in the ideal state by the Epstein frame method, etc.. It is free from the stress and strain associated with motor manufacturing (punching; fixing by caulking, welding, gluing or bolting; winding, press-fitting or shrink-fitting into the frame, etc.) and is also free from deterioration of magnetic properties due to waveform distortion of the exciting current. Although magnetic measurements and magnetic field analyses considering processing strain in the motor manufacturing process have been carried out recently[2–7], further improvement in the accuracy of electromagnetic field analyses is expected from local measurement and visualization of the magnetic flux density, iron loss, stress, etc. in the motor core state. Therefore, in order to measure the local magnetic flux and field strength of motor stator cores, JFE Techno-Research Corporation introduced techniques for local magnetic measurement using the needle probe method (distance between probes: 3.5 mm) and a miniature H-coil (2 mm × 2 mm), which enable nondestructive measurement of non-oriented electrical steel sheets with an insulation coating, and investigated the effects of stress and strain induced during motor production on magnetic properties. These techniques and the measurement results are described in Chapter 2.

The permanent magnets used in rotors are also a key magnetic material with importance equal to that of the non-oriented electrical steel sheets used as motor core materials. Since compact size, high output and high efficiency are demanded in drive motors for EV/HEV, Nd-Fe-B sintered magnets are mainly used in this application, as these magnets offer high residual

† Originally published in *JFE GIHO* No. 47 (Feb. 2021), p. 44−49

[*1] Staff Deputy Manager,
Kurashiki Material Performance Evaluation Center,
West Japan Solution Division,
JFE Techno-Research

[*2] Staff Manager,
Kurashiki Material Performance Evaluation Center,
West Japan Solution Division,
JFE Techno-Research

magnetic flux density and coercivity. Because Nd-Fe-B sintered magnets have lower electrical resistivity than ferrite magnets, a remarkable eddy current is generated inside the magnet due to the effects of the inverter carrier waveform and the slot harmonics caused by the rotating machine structure. If the eddy current loss is excessive, deterioration of magnet properties due to the increased magnet temperature caused by Joule heat is a concern. In EV/HEV drive motors, a segmented structure (divided magnet) is sometimes used to reduce this kind of heat generation[8, 9]. In order to understand the loss reduction effect of the divided magnet structure, it is important to evaluate the AC loss of divided Nd-Fe-B sintered magnets quantitatively. This evaluation technique and the analysis results are described in Chapter 3.

In addition to motor downsizing, higher output and higher efficiency, low vibration and reduction of acoustic noise are also important elements for technology development. Since EV/HEV are significantly quieter than conventional internal combustion engine vehicles, other types of vibration and noise which had been hidden by engine noise and vibration may face a problem. For example, vibration and noise caused by electric power steering systems and air-conditioner compressors became relatively conspicuous in EV/HEV. Against this backdrop as well, motor vibration and acoustic noise have received more attention than in the past[10]. Therefore, JFE Techno-Research introduced a three-dimensional vibration acceleration sensor with vibration analysis system to investigate motor vibration and noise. These techniques and the measurement results are described in Chapter 4.

2. Local Magnetic Property Measurement Techniques for Motor Cores

2.1 Purpose

Although the search coil method has been used as a local magnetic flux measurement method for iron cores, it is necessary to drill holes in the steel sheet, which may influence the distribution of magnetic flux density. To avoid this problem, a nondestructive measurement method using needle probes was developed and applied recently[11, 12]. The following represents an example of measurement techniques for local magnetic properties and the measurement results when these techniques were applied to the stator core of a model motor.

2.2 Measurement Method

Figure 1 shows the schematic drawing of measurement of local magnetic properties using the needle probe and H-coil. The local magnetic flux density of the stator core was obtained based on the theory that the induced voltage between the needle probes, which were placed in contact with the steel sheet surface, is equal to the voltage induced by the magnetic flux crossing 1/2 of the area of the cross section enclosed below the probe contact points[13]. Assuming the distance between the two probes was 3.5 mm, the magnetic flux density was calculated by the following equation.

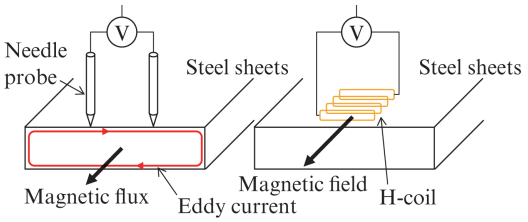

Fig. 1 Method of local magnetic measurement using needle probe and H-coil

$$B_i = (2/S_{Bi}) \int e_{Bi}\, dt \ (i: x, y) \quad \cdots\cdots (1)$$

where, S_{Bi} is the effective area in which the magnetic flux is detected by the probes, and e_{Bi} is the potential difference between the needle probes.

The field strength of the steel sheet surface was calculated by the following equation using the induced voltage of the H-coil, which was placed on the sheet surface.

$$H_i = (1/\mu_0 S_{Hi} N_{Hi}) \int e_{Hi}\, dt \ (i: x, y) \quad \cdots\cdots (2)$$

where, μ_0 is magnetic permeability of vacuum, $S_{Hi}N_{Hi}$ is the effective area turn of the H-coil and e_{Hi} is the output voltage of the H-coil.

Photo 1 shows the needle probe and H-coil and the motor drive system. The motor drive system employs a mechanism in which the tested motor is coupled with an external drive motor by way of a pulley belt, and the tested motor is rotated at the specified speed. The tested motor was a permanent magnet synchronous motor (stator: 18 slots, rotor: 12 poles) with a stator diameter of ϕ200 mm, a rotor diameter of ϕ114 mm and a stack height of 30 mm. The joints between the stator layers were fixed by welding.

2.3 Results and Discussion

Figure 2 shows the magnetic flux density distribution measured by the needle probe technique. The values for each measurement point were the largest absolute values of the magnetic flux vector in one rotation of the rotor. Points with low magnetic flux density were detected in the stator core back part near the welds.

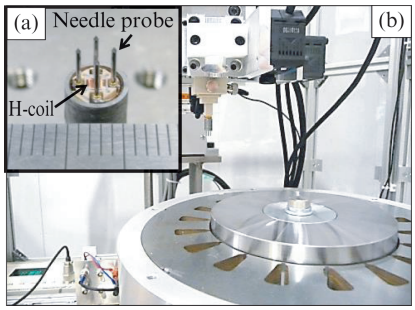

Photo 1 Magnetic sensor with (a) needle probe and H-coil and (b) motor drive system

Figure 3 shows the field strength measured by the H-coil. As in the case of the magnetic flux density distribution, the values for each measurement point were the largest absolute value of the field strength vector in one rotation of the rotor, and the field strength distribution in the stator core back part near the welds was different from that in the non-welded parts.

Figure 4 shows the results of a numerical analysis of the magnetic flux density distribution and the field strength distribution.

In this analysis, the effect of welding on the magnetic properties of the stator core was investigated by using a coupled analysis of heat, structure and the electromagnetic field. When stress was not considered, no changes around welds were found in either the magnetic flux density distribution or the field strength distribution. In contrast, when the residual stress due to welding was considered, deterioration around welds were found and distributions similar to the measured values were obtained for both the magnetic flux density and the field strength.

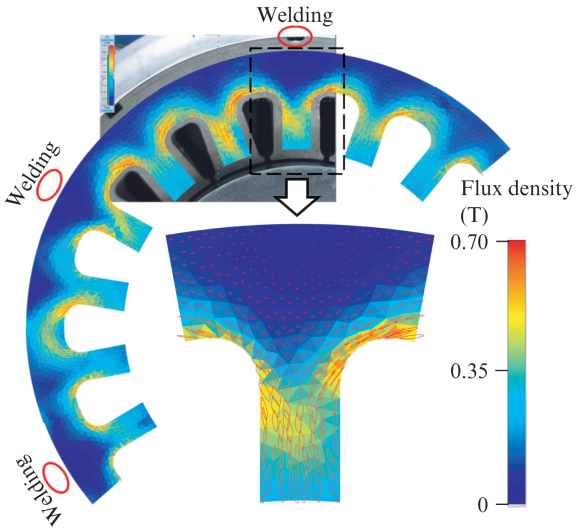

Fig. 2 Magnetic flux density distribution measured by needle probes

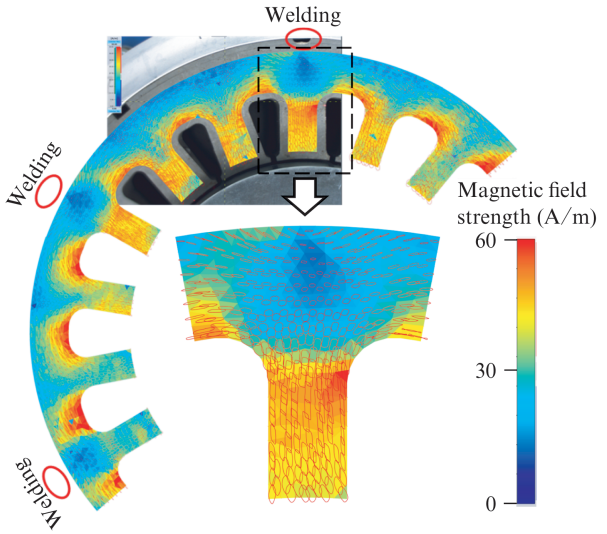

Fig. 3 Magnetic filed strength distribution measured by H-coil

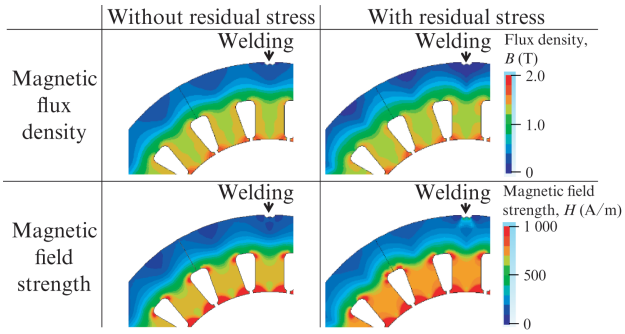

Fig. 4 Results of numerical analysis of magnetic flux density distribution and magnetic field strength distribution

3. AC Loss Measurement Technique for Nd-Fe-B Sintered Magnets

3.1 Purpose

As methods for evaluating eddy current loss in permanent magnets, a method in which AC loss is measured by placing the magnet in a solenoid coil[14], a method in which loss is evaluated by using thermocouples[15], and a method using a test device comprising a closed magnetic circuit[16, 17] have been reported. However, there are few examples of measurement of eddy current loss in divided magnets with the aim of reducing heat generation in permanent magnets.

In the present research, the high frequency iron loss and hysteresis loss of a Nd-Fe-B sintered magnet were measured by using a closed magnetic path AC magnetizing device for AC loss measurement. Eddy current loss was also calculated by subtracting hysteresis loss from total loss, and the effect of division of the Nd-Fe-B sintered magnet on eddy current loss was evaluated. A finite element method (FEM) analysis of eddy cur-

rent loss was also carried out, and the analytical values and measured values were compared.

3.2 Measurement Method

The sample material used here was a Nd-Fe-B sintered magnet (unmagnetized, Ni plated) with dimensions of length 20 mm × width 10 mm × height 7 mm (direction of magnetization: height direction), density of 7 500 kg/m^3 and electrical resistivity of 1.3 $\mu\Omega$-m. **Figure 5** shows the divided structure of the magnet used in the measurements. Insulation treatment was not performed on cut surface between the divided magnets, which were used in the as-divided condition. **Photo 2** shows the closed magnetic path AC magnetizing device for AC loss measurement used in the measurements. Here, an ultra-thin electrical steel sheet with low high-frequency iron loss was used in the yoke that comprises the closed magnetic circuit. The measurements were performed with a maximum magnetic flux density of 0.01 T, 0.05 T or 0.1 T and frequencies in the range from 1 to 8 kHz using sine wave excitation. AC loss was measured with a wattmeter, and the hysteresis loss at each frequency was calculated from the area of the hysteresis loop. The eddy current loss was obtained by deducting the hysteresis loss from AC loss.

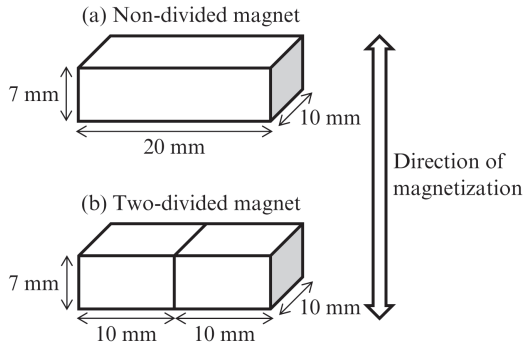

Fig. 5 Schematic diagram of (a) non-divided magnet and (b) two-divided magnet

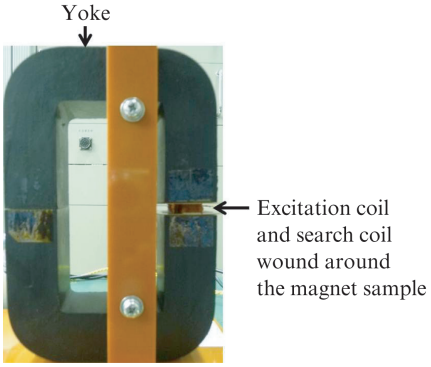

Photo 2 AC magnetizing device for magnet AC eddy current loss measurement

3.3 Measurement Results

Figure 6 shows the relationship between the eddy current loss of the non-divided magnet and the exciting frequency and magnetic flux density. The magnitude of the eddy current loss at 0.1 T was approximately 100 times that at 0.01 T because eddy current loss is proportional to the square of the exciting magnetic flux density.

Figure 7 shows a comparison of the eddy current losses measured in the divided and non-divided magnets. At the exciting frequency of 8 kHz, the eddy current loss of the divided magnet decreased approximately 47% in comparison with the non-divided magnet. Because this measurement was carried out without performing insulation treatment on cut surface between the divided magnets, these results demonstrated that eddy current loss can be reduced greatly simply by dividing the magnet.

3.4 Analysis of Eddy Current Loss of Nd-Fe-B Sintered Magnet

The eddy current loss reduction effect in a divided magnet was analyzed by using the finite element method (FEM). The model used in the eddy current

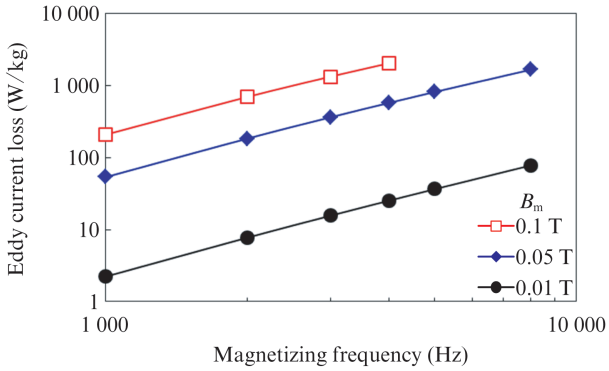

Fig. 6 Eddy current loss measured in non-divided Nd-Fe-B sintered magnet

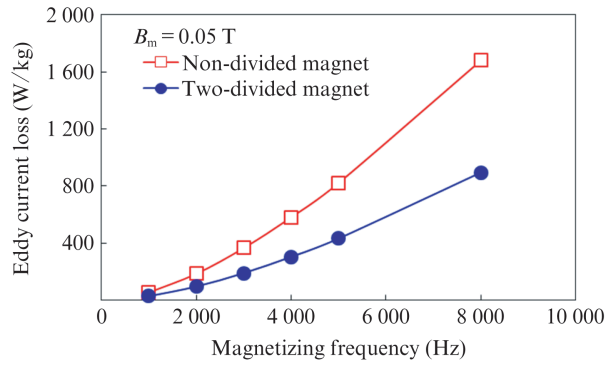

Fig. 7 Comparison of eddy current losses measured in divided and non-divided Nd-Fe-B sintered magnets

loss analysis and the analysis conditions are shown in **Fig. 8** and **Table 1**, respectively. In this analysis, the current amplitude at each frequency was adjusted so that the amplitude of the magnetic flux density passing vertically through the magnet surface was 0.05 T. This analysis was carried out for frequencies of 1 to 8 kHz. The analysis was conducted with a 1/8 model and symmetry was considered.

Figure 9 shows a comparison of the calculated and measured values of eddy current loss in the divided magnet. Although the eddy current loss obtained by the FEM analysis was smaller than the measured values, the results showed comparatively good agreement. Conceivable factors in the divergence between the calculated values and measured values include the effect of loss to the surface treatment layer (Ni plating)[14], the effect of the anisotropy of electrical resistivity, etc.

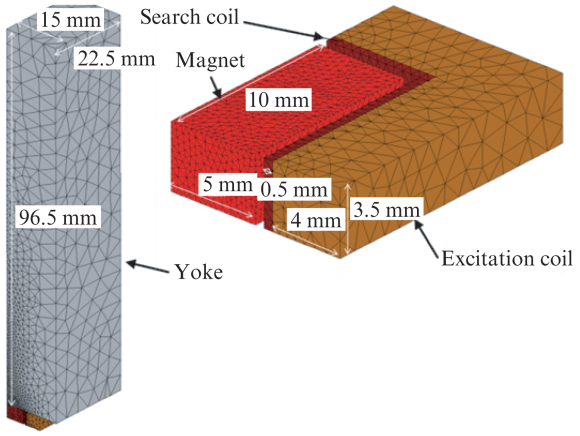

Fig. 8 Analysis model of eddy current loss in divided and non-divided Nd-Fe-B sintered magnets

Table 1 Analysis conditions of eddy current loss in divided and non-divided Nd-Fe-B sintered magnets

Model		1/8
Number of elements		36 704
Density of magnet (kg/m^3)		7 500
Relative permeability of magnet		10
Electric resistivity of magnet ($\mu\Omega$•m)		1.3
Dimension (mm)	Non-divided magnet	20×10×7
	Two-divided magnet	(10+10)×10×7

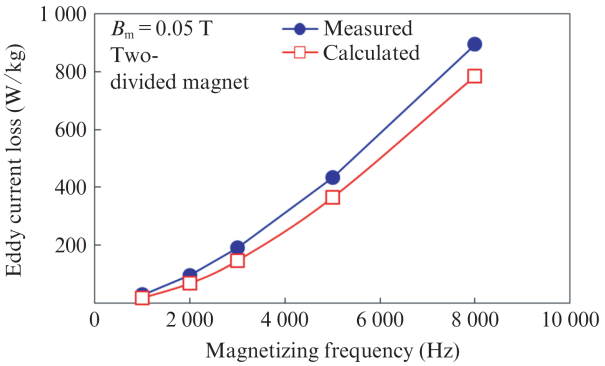

Fig. 9 Comparison of calculated and measured eddy current loss in divided Nd-Fe-B sintered magnet

4. Motor Vibration Evaluation Technique

This chapter introduces an example of a vibration analysis of an interior permanent magnet (IPM) synchronous motor, which is a type of motor used in electrical power steering systems. The motor evaluation system shown in **Photo 3** was used in the evaluation of motor vibration.

The test motor was a 12-pole IPM motor with a stator outer diameter of ϕ156 mm and a stack height of 25 mm as the core dimensions. The driving conditions of the tested motor were a fixed torque of 0.3 Nm and an increase in the revolution at a rate of +5 rpm/s from 500 rpm to 3 000 rpm. The vibration acceleration during this period was measured by using an acceleration sensor mounted on the case of the tested motor, and a tracking analysis was conducted with a FFT analyzer.

The results of the tracking analysis are shown in **Fig. 10**. In Fig. 10, the frequency component of the vibration acceleration measured by the acceleration sensor was mapped with the frequency of the vibration acceleration measured by the acceleration sensor on the abscissa and the revolution of the tested motor on the ordinate. This mapping displayed two distinctive features, as described below.

The first feature is the fact that vibration acceleration increases on the sloping straight lines shown by the red arrows in Fig. 10. Since this indicates that the frequency of vibration acceleration increases in proportion to the revolution of the tested motor, the motor revolution is the direct cause of this vibration. The existence of the multiple lines shown by red arrows is the effect of harmonic components.

The second feature is the increases in vibration acceleration observed in the frequency ranges shown by the blue arrows at the bottom of Fig. 10. These

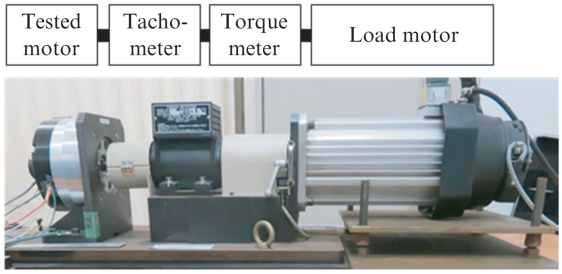

Photo 3 Motor evaluation system

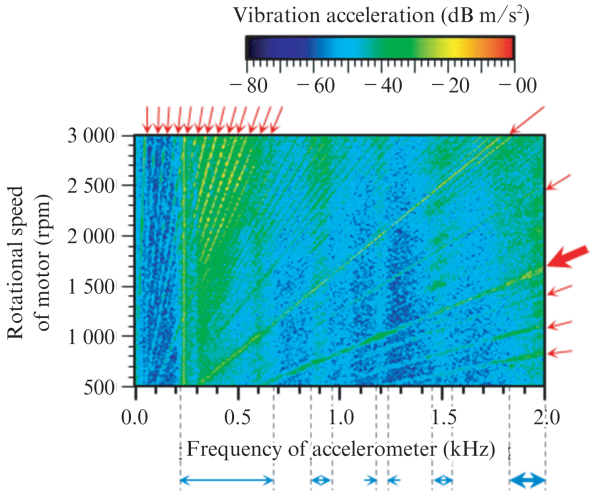

Fig. 10 Tracking analysis of motor vibration

ranges are independent of the motor revolution, and indicate the resonance frequency originating from the mechanical structure of the motor and evaluation system.

Conducting this kind of tracking analysis makes it possible to distinguish and understand the vibration caused directly by motor revolution and the resonance caused by the mechanical structure. Furthermore, vibration becomes particularly large when these two vibration frequencies are superimposed. As shown in **Fig. 11**, the local maximum of overall level of vibration acceleration occurred when the revolution of the motor was around 1 600 rpm. In Fig. 10, the line indicating vibration caused directly by motor revolution (shown by the thick red arrow) and the resonance frequency range caused by the mechanical structure (shown by the thick blue arrow) at 1.8 to 2.0 kHz on the horizontal axis overlap at around 1 600 rpm. Thus, as the cause of the local maximum of the overall level observed at 1 600 rpm, it is considered that the vibration caused directly by motor revolution was amplified by mechanical resonance.

Figure 12 shows the vibration spectra at the motor revolution speeds of 1 600 rpm and 1 400 rpm. The maximum value of vibration acceleration at 1 400 rpm was −15 dB m/s^2 at around the frequency of 0.85 kHz, but at 1 600 rpm, the maximum was −7 dB m/s^2 at around 1.92 kHz. In other words, the maximum value of the frequency component of vibration acceleration was 8 dB m/s^2 larger at 1 600 rpm than at 1 400 rpm. It is thought that the local maximum value of the overall level in Fig. 11 occurred at 1 600 rpm because the overall level of vibration acceleration generally depends on the maximum value of the frequency component.

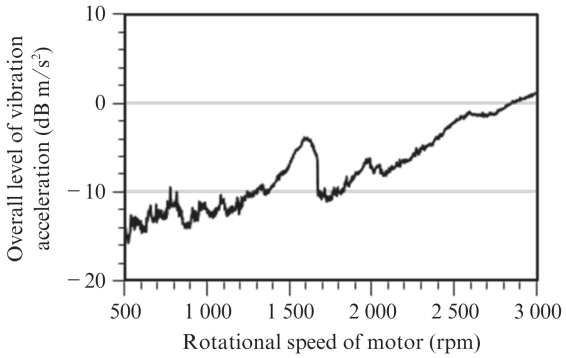

Fig. 11 Tracking analysis of motor vibration

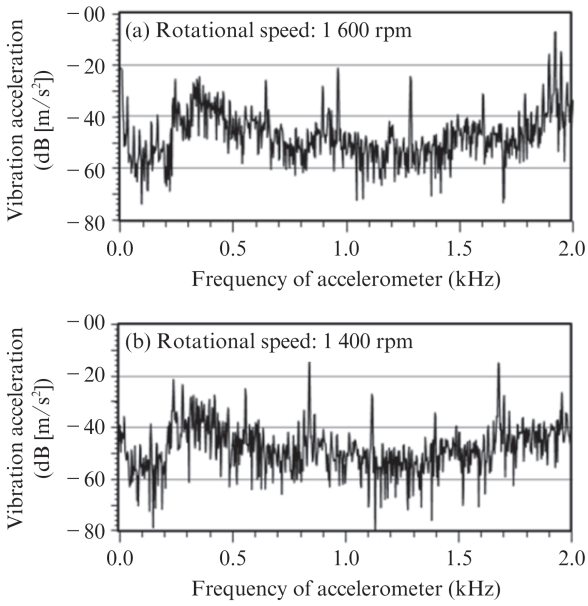

Fig. 12 Vibrational acceleration spectrum

5. Conclusion

As state-of-the-art evaluation and analysis techniques for the magnetic properties of magnetic materials for use in EV/HEV motors, this paper introduced a local magnetic property measurement technique for stator cores, an eddy current loss measurement technique for Nd-Fe-B sintered magnets and a motor vibration analysis technique. As electrification of vehicles progresses, it is thought that higher efficiency will be strongly demanded in EV/HEV motors in the future. JFE Techno-Research will continue to develop magnetic measurement and motor analysis techniques which respond to the increasingly diverse needs of customers, and will provide these techniques as the "Your best partner for *monodzukuri*."

References

1) Oda, Y.; Okubo, T.; Takata, M. Recent Development of Non-Oriented Electrical Steel in JFE Steel. JFE Technical Report.

2016, no. 21, p. 7–13.
2) Senda, K.; Ishida, M.; Nakasu, Y.; Yagi, M. Effect of Shearing Process on Iron Loss and Domain Structure of Non-oriented Electrical Steel. IEEJ Trans, FM. 2005, vol. 125, no. 3, p. 241–246.
3) Kohno, M.; Senda, K.; Hayakawa, Y. Electrical Steels Having Excellent Punchability for Compact and High-functional Automotive Electrical Components. Kawasaki Seitetsu Giho. 2003, vol. 35, no. 1, p. 1–6.
4) Tani, Y.; Daikoku, A.; Nakano, M.; Arita, H.; Yamaguchi, S.; Toide, Y. Magnetic Power Loss Characteristics of Non-oriented Electrical Steel Sheets under Stress. J. Magn. Soc. Jpn. 2006, vol. 30, no. 2, p. 196–200.
5) Senda, K.; Kawano, M.; Ishida, M. Analysis of Core Magnetic Property Deterioration by Interlocking. The Papers of Technical Meeting on Magnetics, IEE Japan. 2005, MAG-05-42, p. 21–26.
6) Kurita, N.; Takahashi, Y.; Fujiwara, K.; Ishihara, Y. Evaluation of Stress-Dependent Magnetic Properties in Non-oriented Electrical Steel Sheets. The Papers of Joint Technical Meeting on Static Apparatus and Rotating Machinery, IEE Japan. 2011, SA-11-25/RM-11-25, p. 61–66.
7) Toda, H.; Oda, Y.; Zaizen, Y. Evaluation and Analysis Methods of Motor characteristics in JFE Steel. JFE Technical Report. 2016, no. 21, p. 28–36.
8) Toda, H.; Wang, J.; Howe, D. Analysis of Motor Loss in Permanent Magnet Brushless Motors. JFE Technical Report. 2005, no. 6, p. 18–23.
9) Murakami, R. Development of magnet application for EV and HEV motors. The Papers of Technical Meeting on Magnetics, IEE Japan. 2015, MAG-15-164, p. 57–60.
10) Yoshikuwa, Y. Journal of the Japan Society of Mechanical Engineers. 2007, vol. 110, no. 1058, p. 62.
11) Senda, K.; Ishida, M.; Honda, A. Direct Measurement of Local Magnetic Properties in Stator Core of Rotating Induction Motor. Kawasaki Seiteysu Giho. 2003, vol. 35, no. 1, p. 16–20.
12) Senda, K.; Ishida, M.; Honda, A.; Ohyama, I. Local Magnetic Properties in Operating Brushless DC Motor. The Papers of Technical Meeting on Rotating Machinery, IEE Japan. 2003, RM-03-42, p. 49–54.
13) Yamaguchi, T.; Imamura, M.; Ishida, M.; Sato, K.; Honda, A.; Yamamoto, T. Analytical Evaluation of the Accuracy of Localized magnetic Flux Measurement by the Stylus Probe Method. T. IEE Japan, 1995, vol. 115-A, no. 1, p. 50–57.
14) Itoh, K.; Hashiba, Y.; Sakai, K.; Yagisawa, T. The A. C. Losses of the Rare-earth Permanent Magnets. T. IEE Japan, 1998, vol. 118-A, no. 2, p. 182–187
15) Aoyama, A.; Ohashi, K.; Miyata, K. Experiment and Analysis of Eddy Current Loss in Permanet Magenet under Alternating Magnet Field. The Paper of Technical Meeting on Rotating Machinery, IEE Japan, 2002, RM-02-135, p. 13–18
16) Kanazawa, S.; Takahashi, N.; Kubo, T. Measurement and Analysis of AC Loss of NdFeB Sintered Magnet. IEEJ Trans. FM, 2004, vol. 124-A, no. 10, p. 869–875.
17) Shimizu, O.; Fujimoto, H.; Nakada, T.; Yoneyama, K.; Takeda, K.; Enokido, Y. Eavluation for theLoss of Permanent Magnet by Actual Measurement and Magnetic Field Analysis. National Convention record I. E. E. Japan, Industry Applications Society. 2019, no. 4–5, p. 99–102.